A Novel Motion Compensation Approach for Airborne Spotlight SAR of High-Resolution and High-Squint Mode

Letian Zeng, Yi Liang, Mengdao Xing, *Member, IEEE*, Yuanyuan Huai, and Zhenyu Li

***Abstract*—This letter proposes a new motion compensation approach for high-squint and high-resolution airborne spotlight synthetic aperture radar (SAR) integrated with polar format algorithm (PFA). The motion error is coarsely compensated by means of measuring systems. In PFA, the expressions of the line-of-sight polar interpolation are first explicitly revealed, and the nonsystematic range cell migration (NsRCM) induced by residual motion error is also corrected, which paves the way for autofocus application. After the NsRCM correction, the enhanced total least square estimator-based phase adjustment by contrast enhancement (PACE) algorithm is considered to account for the residual phase errors extended to the range-dependent case. The processing results of airborne SAR real data are presented to demonstrate the validity of the proposed algorithm.**

***Index Terms*—Enhanced total least square (ETLS), high squint and high resolution, motion compensation (MoCo), polar format algorithm (PFA), spotlight synthetic aperture radar (SAR).**

I. Introduction

SPOTLIGHT synthetic aperture radar (SAR) [1] is an indispensable remote sensing system because of its capacity to obtain high-resolution microwave images, breaking the limitations of antenna length on the azimuth resolution. The highly squinted mode, with squint angles generally greater than 40°, has a potential to increase the flexibility of spotlight SAR in the sense that it can provide information about the unilluminated area in the broadside mode and revisits the particularly interesting area, which cannot be reached instantly by a radar. However, due to the presence of atmospheric turbulence and carrier vibration, raw airborne SAR data are affected by deviations of the platform from an ideal straight flight track, which will significantly degrade the final image quality [2]–[4]. To restrict motion error to an acceptable level, effective motion compensation (MoCo) strategy [5], [6] must be involved in the raw data processing stage, producing impressive reconstructions of the error-corrupted image.

Besides a large range cell migration (RCM), special factors should be considered in highly squinted spotlight SAR data processing. First, the raw signal azimuth bandwidth is, in the spotlight case, generally much greater than the pulse repetition frequency (PRF), which implies that data processing carried out in the Fourier domain cannot be directly implemented on the full aperture because of the consequential azimuth spectrum folding effect [7]. In addition, in the highly squinted mode, motion error caused by serious trajectory deviations will exhibit strong range-dependent effects in the phase errors. Conventional autofocus techniques [4] should be modified to correct spatially variant phase errors that are beyond the capability of the navigation system.

Up to now, several data-driven MoCo approaches have been proposed to deal with motion error in highly squinted data processing for spotlight mode. In [8], a squinted phase gradient autofocus (PGA) algorithm is proposed, which is combined into the omega-K image formation and accounts for the azimuth-dependent quadratic phase due to a high squint angle. Unfortunately, sophisticated interpolators and a high PRF normally lead to a great computation complexity, and interpolators are not as accurate as phase multiplication. Another method presented in [9] is based on the known structure of the range-independent phase error: the 1-D phase error is directly estimated and then mapped into the 2-D phase error under the polar format algorithm (PFA) to achieve an accurate 2-D autofocus.

This study starts with the squinted PFA with motion errors, which is presented to lay the foundation of the new MoCo scheme. First, a coarse MoCo is proposed. After the nonsystematic RCM (NsRCM) correction, the enhanced total least square (ETLS) estimator-based phase adjustment by contrast enhancement (PACE) algorithm is described using a detailed mathematical analysis and applied for spatially variant phase error compensation with high accuracy and efficiency. Finally, real-data experiments demonstrate the performance of the presented scheme.

II. Algorithm of Squinted PFA Imaging With Motion Errors

The squinted spotlight data acquisition of SAR in the conical coordinate system is illustrated in Fig. 1, in which the dotted line denotes the nominal flight trajectory and the solid line denotes the real path of the SAR platform. Assume that the illuminated area is absolutely flat without topography. In the ideal case, the antenna phase center (APC) moves straight along the X-axis (the azimuth direction) with constant velocity v, the radar beam operates in the squint angle θ_s, and the moment corresponding to the center of the synthetic aperture is at slow time $t_m = 0$. The coordinates of the scene center O and

Manuscript received September 1, 2015; revised October 15, 2015 and December 3, 2015; accepted January 9, 2016. Date of publication February 8, 2016; date of current version February 24, 2016. This work was supported in part by the National Nature Science Foundation of China under Grants 61222108 and 61301293 and in part by the Fundamental Research Funds for the Central Universities under Grant K5051302046.

The authors are with the National Laboratory of Radar Signal Processing, Xidian University, Xi'an 710071, China (e-mail: xmd@xidian.edu.cn).

Color versions of one or more of the figures in this paper are available online at http://ieeexplore.ieee.org.

Digital Object Identifier 10.1109/LGRS.2016.2517099

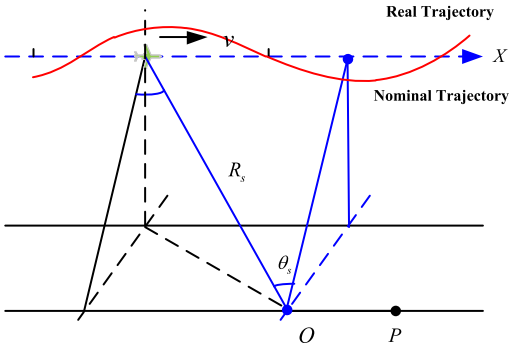

Fig. 1. Geometry of squinted SAR data acquisition.

an arbitrary target point P within the illuminated area are $(R_s \sin\theta_s, R_s \cos\theta_s)$ and $(R_s \sin\theta_s + x, R_s \cos\theta_s + y)$, respectively. However, the irregular motion of the SAR platform caused by atmosphere turbulence as well as its own vibration yields platform trajectory deviations. Considering the presence of the motion errors, the actual instantaneous range of APC from P can be written as

$$R(X;x,y) = R_n(X;x,y) + \Delta R(X) \tag{1}$$

where $R_n(X;x,y) = \sqrt{(X - R_s\sin\theta_s - x)^2 + (R_s\cos\theta_s + y)^2}$ depicts the nominal instantaneous range between the APC and P, $X = vt_m$ signifies the instantaneous azimuth position of the APC in the ideal case, and $\Delta R(X)$ defines the motion error.

Suppose the radar transmits a linear frequency modulated signal, and the received radar echo is given by

$$s(\tau, X; x, y) = \sqrt{\sigma} \cdot \text{rect}\left[\frac{\tau - \Delta\tau}{T_p}\right] a_a(X) \cdot \exp\left[j\pi\gamma(\tau - \Delta\tau)^2\right] \cdot \exp[-j2\pi f_c \cdot \Delta\tau] \tag{2}$$

where σ gives the intensity of the radar echo; $\text{rect}[\tau] = \begin{cases} 1, & |\tau| \le (1/2) \\ 0, & \text{else} \end{cases}$, τ is the range fast time; T_p denotes the duration of the pulse; f_c signifies the carrier frequency and γ is the chirp rate; $a(X)$ represents the azimuth window function; $\Delta\tau = 2R(X;x,y)/c$ describes the actual two-way time delay between the APC and P; and c is the speed of light.

After fast Fourier transform (FFT) with respect to τ in (2), matched filtering and azimuth dechirp are performed by multiplying the phase terms $\exp[j\pi f_r^2/\gamma] \cdot \exp[j \cdot k_r \cdot R_a(X)]$, which yields

$$\begin{aligned} S(k_r, X) =& \text{rect}\left[\frac{k_r - 4\pi f_c/c}{4\pi B_r/c}\right] \\ & \cdot \exp\left[-j \cdot k_r \cdot (R_n(X;x,y) - R_a(X))\right] \\ & \cdot \exp\left[-jk_r \cdot \Delta R(X)\right] \\ \approx& \text{rect}\left[\frac{k_r - 4\pi f_c/c}{4\pi B_r/c}\right] \\ & \cdot \exp\left[-j \cdot k_r \cdot \frac{R_s\cos\theta_s}{\sqrt{(X - R_s\sin\theta_s)^2 + (R_s\cos\theta_s)^2}} \cdot y\right] \\ & \cdot \exp\left[+j \cdot k_r \cdot \frac{X - R_s\sin\theta_s}{\sqrt{(X - R_s\sin\theta_s)^2 + (R_s\cos\theta_s)^2}} \cdot x\right] \\ & \cdot \exp\left[-jk_r \cdot \Delta R(X)\right] \end{aligned} \tag{3}$$

where $k_r = 4\pi(f_c + f_r)/c$ means the range wavenumber, f_r is the range frequency, and B_r describes the bandwidth of the transmitted signal; $R_a(X) = \sqrt{(X - R_s\sin\theta_s)^2 + (R_s\cos\theta_s)^2}$ corresponds to the nominal instantaneous range from APC to O. The second-order as well as higher order phase terms of $R_n(X;x,y) - R_a(X)$ are omitted in the assumption of strictly planar wave fronts. The PFA foresees two resampling operations, the first one in range and the second in azimuth to convert the input signal to the uniformly sampled data on a polar grid. Combined with the highly squinted SAR case, the line-of-sight (LOS) polar interpolation (LOSPI) method is employed to utilize the spectrum information contained in the signal to full extent [4]. Consequently, the range resampling process can be formulated as

$$\begin{aligned} k_y &= \frac{4\pi(f_c + f_r)}{c}\cos(\theta_u - \theta_s) \\ &= \frac{4\pi(f_c + f_r)}{c} \cdot \frac{R_s - X\sin\theta_s}{\sqrt{(X - R_s\sin\theta_s)^2 + (R_s\cos\theta_s)^2}} \end{aligned} \tag{4}$$

where $\theta_u = \cos^{-1}(R_s\cos\theta_s / \sqrt{(X - R_s\sin\theta_s)^2 + (R_s\cos\theta_s)^2})$ denotes the instantaneous squint angle of the APC with respect to O and satisfies the condition $|\theta_u - \theta_s| \le \theta_{\text{bw}}/2$ (θ_{bw} is the beamwidth). Subsequently, azimuth resampling, a nonuniform-to-uniform operation, is applied on a pulse-by-pulse basis as

$$k_x = -k_y \cdot \tan(\theta_u - \theta_s) = k_y \cdot \frac{X\cos\theta_s}{R_s - X\sin\theta_s}. \tag{5}$$

By substituting (4) and (5) into (3), we have

$$\begin{aligned} S_{\text{PR}}(k_x, k_y; x, y) \approx& \text{rect}\left[\frac{k_y - k_0}{4\pi B_r/c}\right] \\ & \cdot \exp\left[j \cdot k_x \cdot (x\cos\theta_s - y\sin\theta_s)\right] \\ & \cdot \exp\left[-j \cdot k_y \cdot (x\sin\theta_s + y\cos\theta_s)\right] \\ & \cdot \exp\left[-j \cdot \vartheta(k_x, k_y)\right] \end{aligned} \tag{6}$$

where $\vartheta(k_x, k_y) = \sqrt{k_x^2 + k_y^2} \cdot \Delta R(X^*) \approx k_y \cdot \Delta R(X^*)$ represents the uncompensated phase error, whose form has been changed by polar reformatting and $X^* = k_x R_s/(k_x\sin\theta_s + k_y\cos\theta_s)$ indicates the new azimuth position.

Using a Taylor series expansion on $k_y = k_0 = 4\pi f_c/c$, $\vartheta(k_x, k_y)$ has leading terms

$$\vartheta(k_x, k_y) \approx k_0 \cdot \Delta R\left(X_0^*\right) + \Delta k_y \cdot \Delta r_{\text{NsRCM}} \tag{7}$$

where $X_0^* = X^*{}_{k_y = k_0} = k_x \cdot R_s/(k_x\sin\theta_s + k_0\cos\theta_s)$, $\Delta k_y = k_y - k_0$, and the NsRCM can be approximated as

$$\Delta r_{\text{NsRCM}} \approx \Delta R\left(X_0^*\right) - X_0^* \cdot \Delta R'\left(X_0^*\right) \tag{8}$$

where $\Delta R'(X_0^*)$ is the value of the first-order derivative of $\Delta R(X^*)$ at $X^* = X_0^*$. Omitting the constant terms, we can rearrange (6) as

$$\begin{aligned} S_{\text{PR}}(k_x, \Delta k_y; x, y) \approx& \text{rect}\left[\frac{\Delta k_y}{4\pi B_r/c}\right] \\ & \cdot \exp\left[j \cdot k_x \cdot (x\cos\theta_s - y\sin\theta_s)\right] \\ & \cdot \exp\left[-j \cdot \Delta k_y \cdot (x\sin\theta_s + y\cos\theta_s)\right] \\ & \cdot \exp[-j \cdot \Delta k_y \cdot \Delta r_{\text{NsRCM}}] \\ & \cdot \exp\left[-j \cdot k_0 \cdot \Delta R\left(X_0^*\right)\right]. \end{aligned} \tag{9}$$

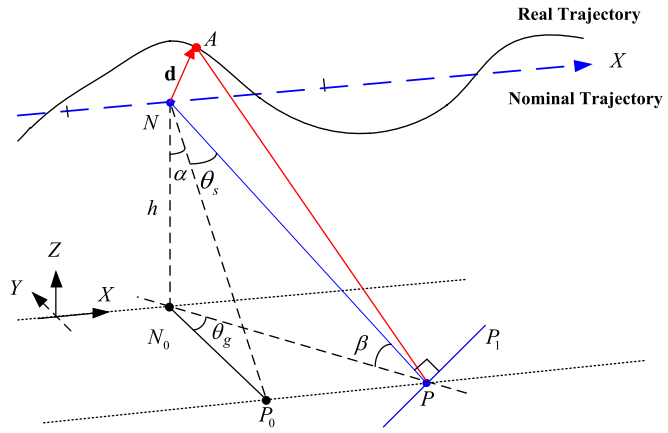

Fig. 2. Squinted SAR motion geometry.

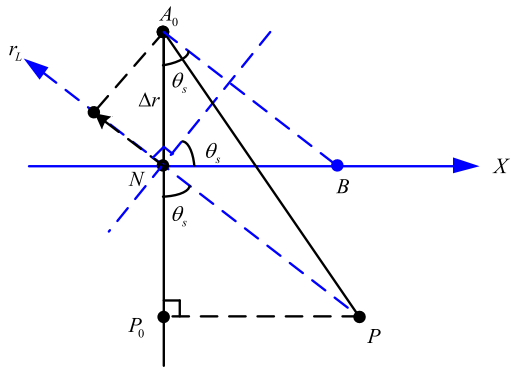

Fig. 3. Off-track error in slant plane.

At this stage, the motion error is expected to be compensated further. That is, in the highly squinted spotlight mode, the residual range error is not only introduced by the residual motion error itself but also caused by the influence of polar reformatting, which changes the shape as well as the magnitude of the residual error. After inverse FFT (IFFT) is applied with respect to Δk_y and FFT to k_x, the focused image is obtained, where LOSPI is used to implement $\begin{bmatrix} x' \\ y' \end{bmatrix} = \begin{bmatrix} \cos\theta_s & -\sin\theta_s \\ \sin\theta_s & \cos\theta_s \end{bmatrix} \cdot \begin{bmatrix} x \\ y \end{bmatrix}$, i.e., a rotation of the output image by θ_s.

III. MoCo Algorithm

The proposed MoCo procedure mainly consists of two parts: coarse compensation and fine compensation. The latter can also be composed of NsRCM correction and ETLS estimator-based PACE algorithm, obtaining a sound result for removing the residual motion error.

A. Coarse Compensation

Let us refer to Fig. 2, where the squinted SAR motion geometry is depicted. The APC moves in the increasing X-axis, while the Y- and Z-axes, vertical to each other, lie in the plane perpendicular to the X-axis. The radar beam operates at a squint angle θ_s, and the moment corresponding to the center of the synthetic aperture defines the azimuth slow time $t_m = 0$. θ_g refers to the projection angle of θ_s onto the ground. During data acquisition, the APC deviates from the nominal position N on the ideal flight track by the vector $\mathbf{d} = (\Delta x(t_m), \Delta y(t_m), \Delta z(t_m))$. The ideal position N and the actual position A at t_m are $(vt_m, 0, h)$ and $(vt_m + \Delta x(t_m), \Delta y(t_m), h + \Delta z(t_m))$, respectively.

Different from the broadside case, the normal plane NN_0P_0, with N_0 as the projection of N onto the ground and the incident angle α, no longer coincides with the plane NN_0P in which the beam center lies with the depression angle β. Accordingly, the effects of the APC deviation in NN_0P_0 on the slant range error change. Herein, one ignores the error perpendicular to the slant plane NP_0P that has no consequences for the SAR focusing procedure [4]. The MoCo can only be performed in the LOS beam-center direction (the direction of wave propagation) and in the azimuth direction (along the X-axis). Therefore, the deviation $\mathbf{d}$ can be first decomposed into $\Delta x(t_m)$ in the X-axis and $\Delta r(t_m)$ as the projection of $(0, \Delta y(t_m), \Delta z(t_m))$ in NN_0P_0 along the direction from P_0 to N, ignoring the component vertical to $\mathbf{NP_0}$. As Fig. 3 shows, we denote $|\mathbf{A_0N}| = \Delta r(t_m)$, which results in a time delay error of the received echo and can be calculated from the projections of $\Delta y(t_m)$ and $\Delta z(t_m)$ onto $\mathbf{NP_0}$, which leads to $\Delta r(t_m) = \Delta y(t_m) \cdot \sin\alpha + \Delta z(t_m) \cdot \cos\alpha$. However, the time delay error is actually linked to the range error $\Delta r_L(t_m) = \Delta r(t_m) \cdot \cos\theta_s$, which lies in the LOS direction.

After range compression and omission of the constant terms, the radar echo becomes

$$s(\tau, X; x, y) = \sin c\left[B_r \cdot (\tau - \tau_0 - \Delta\tau_e)\right] \cdot a_a(X) \cdot \exp\left[-j2\pi f_c \cdot (\tau_0 + \Delta\tau_e)\right] \quad (10)$$

where $\tau_0 = 2 \cdot |\mathbf{NP}|/c$ and $\Delta\tau_e \approx 2\Delta r_L(t_m)/c$ denote the time delays of the ideal range and the corresponding range error, respectively. Thus, the phase compensation function has the form $H_{\text{pha}}(t_m) = \exp(j \cdot 2\pi f_c \cdot \Delta\tau_e)$. Multiplying $H_{\text{pha}}(t_m)$ by (10) and performing FFT with respect to τ, we have

$$s(f_r, X; x, y) = \text{rect}\left[\frac{f_r}{B_r}\right] \cdot a_a(X) \cdot \exp[-j2\pi f_c \cdot \tau_0] \cdot \exp[-j2\pi f_r \cdot \tau_0] \cdot \exp[-j2\pi f_r \cdot \Delta\tau_e]. \quad (11)$$

In Fig. 3, to move the actual position A_0 to the nominal position N, we can first move A_0 to B in the LOS direction via multiplying (11) by the envelop-error compensation function $H_{\text{env}}(f_r, t_m) = \exp(j \cdot 2\pi f_r \cdot 2\Delta r(t_m)/(c\cos\theta_s))$, which yields

$$s(f_r, X; x, y) = \text{rect}\left[\frac{f_r}{B_r}\right] \cdot a_a(X) \cdot \exp[-j2\pi(f_c + f_r) \cdot \tau_0] \cdot \exp\left[j4\pi f_r \cdot \Delta x_0 \sin\theta_s/c\right] \quad (12)$$

where $\Delta x_0 = \Delta r(t_m)\tan\theta_s = |\mathbf{BN}|$ can be compensated in the azimuth direction by interpolation and resampling, shifting B to N. As a matter of fact, the correction of Δx_0 and the along-track error $\Delta x(t_m)$ can be carried out together with one interpolation and resampling step.

B. NsRCM Correction

After the coarse MoCo, the remaining motion error still manifests itself as NsRCM induced by polar reformatting, which would degrade the image focusing if not compensated. An effective method to resolve this problem is detailed in [9] with range-compressed and coarser-resolution data by the conventional autofocus algorithm. Accordingly, the influence of the NsRCM on the signal envelop is removed by multiplying (9) by $H_{\text{NsRCM}}(k_x, \Delta k_y) = \exp[j \cdot \Delta k_y \cdot (\Delta R(X_0^*) - X_0^* \cdot \Delta R'(X_0^*))]$ before range IFFT is utilized.

C. ETLS Estimator-Based PACE

In this part, it is assumed that the residual motion error is small enough to be considered as a phase error. For a target P in the ith range bin ($i = 1, 2, \ldots, M$, M denotes the number of the range bins), its residual phase error is essentially range-dependent and can be formulated as

$$\begin{aligned}\Delta\varphi_i(t_m) &= -\frac{4\pi}{\lambda}\Delta r_i(t_m)\cdot\cos\theta_s \\ &= -\frac{4\pi}{\lambda}\left(\Delta y(t_m)\cdot\cos\theta_g\cdot\cos\beta_i + \Delta z(t_m)\cdot\sin\beta_i\right)\end{aligned} \tag{13}$$

where $\beta_i = \sin^{-1}(h/R_i)$ and R_i are the depression angle and the slant range of the ith range cell, respectively.

For the squinted cases, the range-dependent phase errors for the targets in the direction of the range walk in the horizontal plane are considered the same [6], implying that the range-invariant direction of phase errors coincides with the direction perpendicular to the LOS (as the solid line PP_1 shows in Fig. 2), consistent with the result accomplished by LOSPI and NsRCM correction in Section III-B. The phase-error compensation procedure of the phase history data can be modeled as

$$\boldsymbol{\varphi} = \mathbf{HD} + \mathbf{e} \tag{14}$$

where $\mathbf{H} = -(4\pi/\lambda)\begin{bmatrix}\cos\beta_1\cos\theta_g & \sin\beta_1 \\ \cos\beta_2\cos\theta_g & \sin\beta_2 \\ \vdots & \vdots \\ \cos\beta_M\cos\theta_g & \sin\beta_M\end{bmatrix}$ is the parameter matrix, $\mathbf{D} = \begin{bmatrix}\Delta y_1 & \Delta y_2 & \cdots & \Delta y_Q \\ \Delta z_1 & \Delta z_2 & \cdots & \Delta z_Q\end{bmatrix}$ signifies the off-track error matrix of the SAR platform, $\boldsymbol{\varphi}$ denotes the phase error, $\mathbf{e}$ describes the error matrix of $\boldsymbol{\varphi}$, and Q is the number of the radar pulses. In fact, $\mathbf{H}$ varies with the topography of the terrain, the deviations and vibrations of the SAR platform. Thus, we can employ the total least square (TLS) method to find a new subspace to effectively balance between $\mathbf{H}$ and $\boldsymbol{\varphi}$. Then, we have

$$[\mathbf{H} \quad \boldsymbol{\varphi}] = \mathbf{U}\sum\mathbf{V}^T \quad \mathbf{U} = [\mathbf{U_r} \quad \mathbf{u}] \tag{15}$$

where $\mathbf{U}\sum\mathbf{V}^T$ is the singular value decomposition of the matrix $[\mathbf{H} \quad \boldsymbol{\varphi}]$, $\mathbf{U_r}$ is constructed from the left singular vectors that correspond to the larger singular values of $[\mathbf{H} \quad \boldsymbol{\varphi}]$ with rank r, and $\mathbf{U_r^T U_r} = \mathbf{I_r}$. Then, the TLS solution of (14) becomes [10]

$$\boldsymbol{\Psi_e} = \left(\mathbf{H}^T\mathbf{P_r}\mathbf{H}\right)^{-1}\mathbf{H}^T\mathbf{P_r}\boldsymbol{\varphi} \tag{16}$$

where $\mathbf{P_r} = \mathbf{U_r}\mathbf{U_r^T}$ is obtained from the left singular vectors of $[\mathbf{H} \quad \boldsymbol{\varphi}]$. Moreover, we can find that $\mathbf{P_r}$ satisfies the following expressions $\mathbf{P_r^2} = \mathbf{U_r}\mathbf{U_r^T}\cdot\mathbf{U_r}\mathbf{U_r^T} = \mathbf{U_r}\mathbf{U_r^T} = \mathbf{P_r}$ and $\mathbf{P_r^T} = \left(\mathbf{U_r}\mathbf{U_r^T}\right)^T = \mathbf{U_r}\mathbf{U_r^T} = \mathbf{P_r}$. That is, $\mathbf{P_r}$ is an orthogonal projector. Therefore, (16) can be rearranged into

$$\boldsymbol{\Psi_e} = \left(\mathbf{H}^T\mathbf{P_r}\cdot\mathbf{P_r^T}\mathbf{H}\right)^{-1}\mathbf{H}^T\mathbf{P_r}\cdot\mathbf{P_r^T}\boldsymbol{\varphi} = \left(\mathbf{H_1^T H_1}\right)^{-1}\mathbf{H_1^T}\boldsymbol{\varphi_1} \tag{17}$$

where $\mathbf{H_1} = \mathbf{P_r^T H}$ and $\boldsymbol{\varphi_1} = \mathbf{P_r}\boldsymbol{\varphi}$. In fact, $\boldsymbol{\Psi_e}$ is the least square solution of the linear equation $\boldsymbol{\varphi_1} = \mathbf{H_1 D} + \mathbf{e_1}$, where

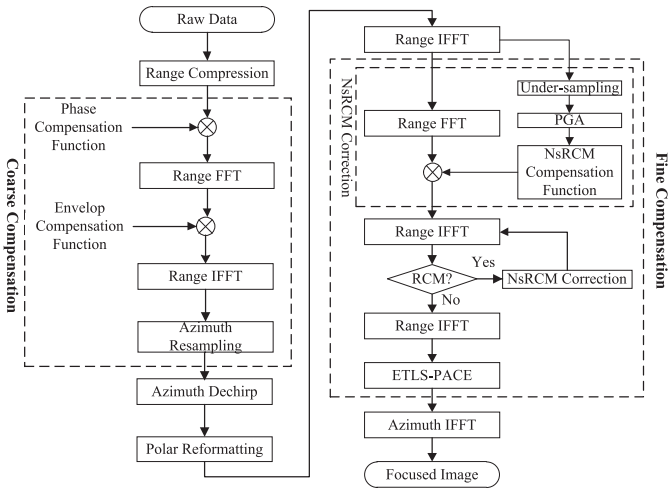

Fig. 4. Flowchart of the proposed algorithm.

$\mathbf{e_1}$ is the error matrix of $\boldsymbol{\varphi_1}$ and its variance is described as $\mathrm{var}(\boldsymbol{\varphi_1}) = \mathrm{var}(\mathbf{H_1 D}) + \mathrm{var}(\mathbf{e_1}) = \mathrm{var}(\mathbf{e_1})$ [10]. Because the phase error of each range bin is sensitive to strong noise and clutter, the precision of the estimate is not guaranteed. Hence, (17) does not differentiate yet between high-precision and low-precision estimates. To achieve this, a global optimization can be obtained via ETLS estimation by assigning a weight to each range bin data

$$\boldsymbol{\Psi_e} = \left(\mathbf{H_1^T R_1^{-1} H_1}\right)^{-1}\mathbf{H_1^T R_1^{-1}}\boldsymbol{\varphi_1} \tag{18}$$

where $\mathbf{R_1} = \mathrm{diag}[\mathrm{var}(\mathbf{e_1})]$ is a weighting matrix, $\boldsymbol{\varphi_1} = [\boldsymbol{\varphi_1}(1,:) \quad \boldsymbol{\varphi_1}(2,:) \quad \cdots \quad \boldsymbol{\varphi_1}(M,:)]^T$ is the estimated phase error matrix, and $\boldsymbol{\varphi_1}(i,:)$ is the phase error estimate achieved from the ith range bin data, which can be estimated by a highly accurate and computationally efficient autofocus algorithm—PACE [11]. Finally, the corresponding horizontal and vertical components of the motion deviations, $\mathbf{D_y}$ and $\mathbf{D_z}$, are determined by $\begin{bmatrix}\mathbf{D_y} \\ \mathbf{D_z}\end{bmatrix} = (\lambda/4\pi)\boldsymbol{\Psi_e}$. After the phase error compensations associated with $\mathbf{D_y}$ and $\mathbf{D_z}$, we can achieve a properly focused image.

The flowchart of the whole processing chain is illustrated in Fig. 4.

IV. Real-Data Experiment

In this part, we perform a real-data experiment to investigate the feasibility of the proposed autofocus scheme to compensate both the range-independent and spatially variant motion errors. The data set is acquired by an X-band SAR working in spotlight mode with a squinted angle being about 42°. The transmitted signal bandwidth is 600 MHz, and the synthetic aperture length is about 1.05 km. The height of the SAR platform is about 5.7 km, and the range to the scene center is 15.15 km. The slant plane image is 2 × 1 km with a nominal range and azimuth resolution of 0.25 × 0.3 m. The SAR system is merely equipped with a gyroscope and a GPS system. The altitude control is at an accuracy of 3 m, the gyroscope provides motion information at the frequency of 12.5 Hz, and its GPS positioning accuracy is 10 m, which is insufficient for the generation of high-quality

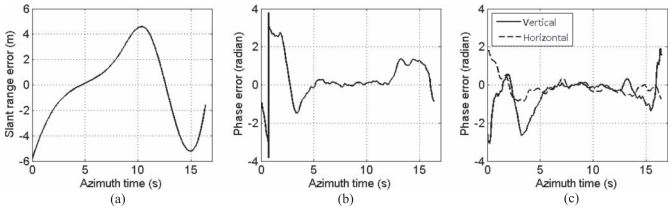

Fig. 5. (a) Slant range error obtained by the measuring system. (b) Phase error estimated by the reference algorithm. (c) Horizontal and vertical components of the phase error estimated by the proposed algorithm.

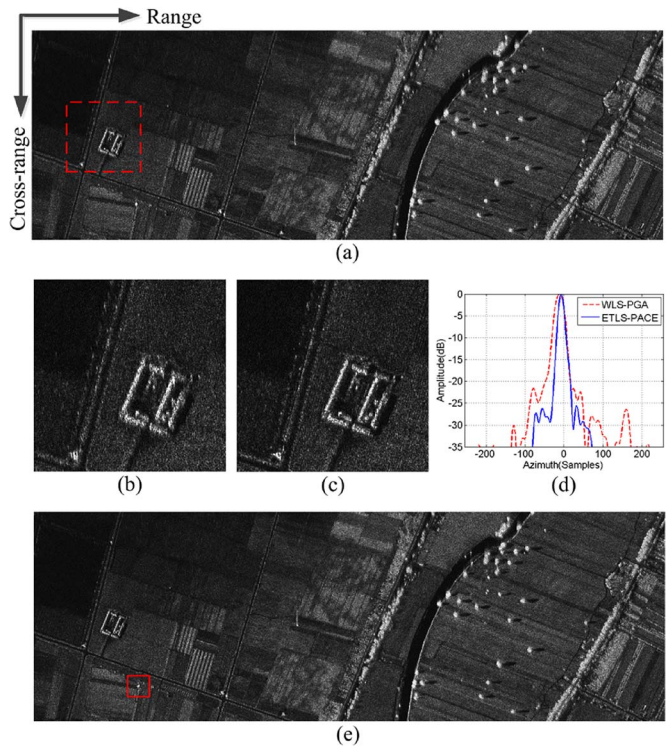

Fig. 6. Comparison of the results for real SAR data set. (a) Result using the reference algorithm. (b) Expanded local figure from (a). (c) Magnified local figure with the proposed algorithm. (d) Comparison of IRF. (e) Result using the proposed algorithm.

imagery. Herein, the acquired data are first compensated by the proposed algorithm. As a reference algorithm, the ETLS-PACE method is substituted with the WLS-PGA method [12] within the proposed algorithm, while the other operations remain unchanged. Both algorithms are executed on a personal computer with Intel Pentium dual-core CPU G630 at 2.7 GHz.

The slant range error obtained by the measuring system is shown in Fig. 5(a), and it is up to about 10 m during data acquisition. The residual phase error estimated by the reference algorithm is illustrated in Fig. 5(b). However, the reference algorithm can only estimate the spatially invariant phase error. The horizontal and vertical components of the phase error extracted by the proposed algorithm are depicted in Fig. 5(c), which can be utilized to correct the essentially range-dependent phase error accurately. The imaging results obtained by the reference algorithm and the proposed algorithm are shown in Fig. 6(a) and (e), respectively. The processing time of the algorithms is about 130 and 107 min in the listed order. The proposed algorithm provides better results with more efficiency than the reference one.

For comparison, in Fig. 6(b) and (c) from the near-range area, we show the magnified local images of the region within the dotted frame obtained with the two algorithms, whose entropies are 12.280 and 12.099, respectively. Clearly, the scenes are more distinguished, and impressive improvement of the image quality is achieved via the proposed algorithm. With regard to a certain target within the solid box, the reference algorithm performs poorly in comparison with the proposed algorithm, as from Fig. 6(d). The experiment confirms that our autofocus approach can provide promising performance in focusing highly squinted spotlight SAR data with equipment of only a medium-accuracy measuring system.

V. Conclusion

This letter has described the difficulties of airborne spotlight SAR focusing in a squinted geometry, taking into account residual motion errors. The proposed approach is capable of efficiently accommodating strong trajectory deviations during squinted spotlight SAR processing, when a medium accuracy navigation system is equipped. It considers the correction of NsRCM induced by the effects of LOSPI on the residual motion error, paving the way for autofocus with the presented ETLS-PACE algorithm. The proposed MoCo scheme is promising for airborne spotlight SAR data processing in the squinted mode. Real high-resolution squinted spotlight SAR data experiments validate the effectiveness of the proposed approach.

References

[1] I. G. Cumming and F. H. Wong, *Digital Processing of Synthetic Aperture Radar Data: Algorithms and Implementation*. Norwood, MA, USA: Artech House, 2005.

[2] H. M. J. Cantalloube and C. E. Nahum, "Multiscale local map-drift driven multilateration SAR autofocus using fast polar format algorithm image synthesis," *IEEE Trans. Geosci. Remote Sens.*, vol. 49, no. 10, pp. 3730–3736, Oct. 2010.

[3] O. O. Bezvesiliniy, I. M. Gorovyi, and D. M. Vavriv, "Estimation of phase errors in SAR data by local-quadratic map-drift autofocus," in *Proc. IEEE 13th IRS*, Warsaw, Poland, 2012, pp. 376–381.

[4] W. G. Carrara, R. S. Goodman, and R. M. Majewski, *Spotlight Synthetic Aperture Radar: Signal Processing Algorithm*. Norwood, MA, USA: Artech House, 1995.

[5] K. A. C. deMacedo, R. Scheiber, and A. Moreira, "An autofocus approach for residual motion errors with application to airborne repeated-pass SAR interferometry," *IEEE Trans. Geosci. Remote Sens.*, vol. 46, no. 10, pp. 3151–3162, Oct. 2008.

[6] G. Xu *et al.*, "Robust autofocusing approach for highly squinted SAR imagery using the extended wavenumber algorithm," *IEEE Trans. Geosci. Remote Sens.*, vol. 51, no. 10, pp. 5031–5046, Oct. 2013.

[7] R. Lanari, M. Tesauro, E. Sansosti, and G. Fornaro, "Spotlight SAR data processing based on a two-step processing approach," *IEEE Trans. Geosci. Remote Sens.*, vol. 39, no. 9, pp. 1993–2004, Sep. 2001.

[8] L. Zhang *et al.*, "Wavenumber-domain autofocusing for highly squinted UAV SAR imagery," *IEEE Sens. J.*, vol. 12, no. 5, pp. 1574–1588, Aug. 2012.

[9] X. Mao, D. Zhu, and Y. D. Zhang, "Knowledge-aided two-dimensional autofocus for synthetic aperture radar," in *Proc. IEEE Int. Radar Conf.*, Ottawa, ON, Canada, 2013, pp. 1–6.

[10] L. L. Scharf, *Statistical Signal Processing, Detection, Estimation, and Time Series Analysis*. Reading, MA, USA: Addison-Wesley, 1991.

[11] J. Kolman, "PACE: An autofocus algorithm for SAR," in *IEEE Int. Radar Conf.*, Arlington, VA, USA, May 2005, pp. 310–314.

[12] W. Ye, T. S. Yeo, and Z. Bao, "Weighted least-squares estimation of phase errors for SAR/ISAR autofocus," *IEEE Trans. Geosci. Remote Sens.*, vol. 37, no. 5, pp. 2487–2494, Sep. 1999.